A Wave Based approach for the dynamic bending analysis of Kirchhoff plates under distributed deterministic and random excitation

Stijn Jonckheere*, Dirk Vandepitte, Wim Desmet

KU Leuven, Dept. of Mechanical Engineering, Celestijnenlaan 300B - box 2420, 3001 Leuven, Belgium

Abstract

For the harmonic analysis of plate bending problems, the Finite Element Method (FEM) is a commonly applied numerical technique. Its element concept with polynomial approximation functions, however, limits its applicable frequency range because of a strongly increasing computational cost. The Wave Based Method (WBM) has can relax this by using wave functions, which satisfy the governing differential equations.

This paper derives two distinct particular solution sets for distributed loads in the WBM. Two numerical validations show the improved efficiency as compared to the FEM. The novel approach is also applied to a plate under a TBL excitation.

Keywords: structural dynamics, plate bending, Kirchhoff theory, Wave Based Method, distributed load, turbulent boundary layer excitation

1. Introduction

The Finite Element Method (FEM) [1] is one of the most commonly applied simulation technologies to predict the behaviour of dynamic systems since it can tackle geometrically complex problems by dividing the problem domain in small elements. Simple polynomial approximation functions are most commonly used within the elements to describe the dynamic field variables. This procedure, involving small elements with polynomial functions is the strength of the FEM, but it also constitutes a limitation. As the frequency increases, the number of elements required to control the

*Corresponding author, Address: KU Leuven - Department of Mechanical Engineering, Celestijnenlaan 300B - box 2420, 3001 Leuven, Belgium, Tel.:+32 16 37 28 32; Fax: +32 16 32 28 38.
E-mail address: Stijn.Jonckheere@kuleuven.be

interpolation and pollution errors increases more than linearly [2, 3, 4]. The increasing model size creates an upper frequency limit above which the computational cost becomes prohibitive. The FEM should thus be considered as a low-frequency technique.

Significant research is performed in order to alleviate these limitations of the FEM. Important to mention are the so-called meshless methods, where the very fine element discretisation is no longer made. Instead, approximation functions with a higher degree of continuity are applied. The application to thin plates can be found in many fields of dynamic analysis: e.g. nonlinear dynamic fracture and crack growth [5, 6], buckling analysis [7, 8] and steady-state linear vibration analysis [9, 10]. Another class of techniques, partly intersecting the class of the meshless methods, is the group of Trefftz-based methods [11, 12]. These methods all apply the same principle; the solution is approximated through a set of so-called Trefftz functions, which inherently satisfy the governing differential equation(s) *a priori* and which may violate conditions at the domain boundary. The best known Trefftz-based methods are the Discontinuous Galerkin Method [13], the Hybrid Trefftz FEM [14], the Method of Fundamental Solutions [15, 16], the Variational Theory of Complex Rays [9, 17], the Ultra-Weak Variational Formulation [18, 19, 20] and the Wave Based Method (WBM) [21], which is the focus of this paper. The key differentiator between these methods is the way in which the boundary and interface conditions are imposed and the specific selection of type of basis functions.

This paper focuses on the Wave Based Method (WBM) [21], which has the potential to alleviate the FEM's frequency limitations for problems of moderate geometrical complexity. As compared to FE models, WB models are much smaller and have a higher convergence rate, which enables faster calculations for the same accuracy or allows going to higher frequencies for the same computational cost. So far, the method has been successfully applied to acoustic problems [22, 23, 24], in-plane membrane [25] and plate bending [10] problems, poro-elastic problems [26, 27] and, in a hybrid sense with the FEM, to fully coupled vibro-acoustic problems with structural [28] and poro-elastic [29] components.

The WBM for plate bending problems forms the starting point of this paper. The research on these problem settings was initiated by Desmet [21]. Vanmaele et al. [10, 30] studied this topic more profoundly. So far, however, the WBM only allows for excitation by a prescribed boundary condition, or excitation by a point force inside the domain. Nevertheless, distributed loads are omnipresent in engineering practise. They can cover a wide range of load profiles, ranging

from loaded patches to full surface distributed loads. In the former case, concentrated loads are distributed over a small but finite area. Depending on the ratio between the patch dimensions and the governing wavelength, the assumption of a localised point force no longer holds. Examples of the latter case are the vibro-acoustic coupled problems and the excitation by a broadband random excitation, such as e.g. a diffuse acoustic field or a turbulent boundary layer (TBL). By virtue of their stochastic nature, these random excitations are only known in statistical terms. They can however be elegantly described in the wavenumber-frequency domain [31]. Whereas the diffuse field models yield accurate results using only a simple expression, the excitation by a TBL is less trivial to model. Corcos [32] developed an empirical model describing the spectrum of the turbulent boundary layer wall pressure. Over the years, improvements have been made, among others by Efimtsov [33] and Chase [34]. Nevertheless the model still stands as a good estimate of the wall pressure fluctuations' so-called convective ridge [35]. An extensive overview of the modelling of turbulent boundary layer spectra can be found in [36].

The topic of distributed loads in the WBM, however, has only briefly been touched on so far. Desmet [21] used the acoustic wave functions as particular solutions to the plate bending problem in order to have fully coupled vibro-acoustic WB models. Jegorovs [37] introduced the use of the Fourier transform for the derivation of particular solutions and applied this to the so-called light diffusion approximation to the transport theory. In this paper, the existing framework of the WBM for plate bending problems is extended with particular solutions which can incorporate the effect of distributed loads in dynamic plate bending problems. Two different approaches are presented. The first one is derived from the integration of the particular solution for a point force over the loaded surface. In the second approach, particular solutions are derived based on a decomposition of the distributed load in the wavenumber domain. Both approaches are validated in terms of efficiency and accuracy.

The paper is organised as follows; Section 2 reviews the mathematical formulations of the plate bending problem, with its governing dynamic equation and boundary conditions. The WBM for plate bending problems is discussed in Section 3. The existing framework is extended with particular solutions for distributed loads in Section 4. Section 5 demonstrates the potential of the developed functions with a number of academic numerical validation examples, both on a simple rectangular plate and on a more complicated shape. Section 6 uses the newly developed particular solutions to compute the response of a plate under a TBL excitation. The paper ends with a general conclusion

on the presented work.

2. Problem definition

Consider a thin flat plate shown in Fig. 1. The steady-state dynamic behaviour can be described by the Kirchhoff theory [38]. According to this thin plate theory, the steady-state out-of-plane displacements $w_z(\mathbf{r})$, with $\mathbf{r} = (x, y)$, are governed by the following fourth order partial differential equation:

$$\mathbf{r} \in \Omega : \nabla^4 w_z(\mathbf{r}) - \left(k_b^s\right)^4 w_z(\mathbf{r}) = \frac{F_z}{D}\delta(\mathbf{r_F}) - \frac{p(\mathbf{r_d})}{D}, \tag{1}$$

where $\nabla^4 = \frac{\partial^4}{\partial x^4} + 2\frac{\partial^4}{\partial x^2 y^2} + \frac{\partial^4}{\partial y^4}$. The structural wavenumber for plate bending k_b^s and the bending stiffness D are defined as:

$$k_b^s = \sqrt[4]{\frac{\rho t \omega^2}{D}}, \tag{2}$$

$$D = \frac{E(1 + \mathrm{j}\eta)t^3}{12(1 - \nu^2)}, \tag{3}$$

with t the thickness of the plate, E the elasticity modulus, η the material loss factor, ν the Poisson coefficient, ρ the material density, $\omega = 2\pi f$ the harmonic pulsation and $\mathrm{j}^2 = -1$. The plate is excited by a normal point force F_z in the point $\mathbf{r_F} = (x_F, y_F)$ and by a distributed normal load $p(\mathbf{r_d})$ on a part Ω^d of the plate surface Ω.

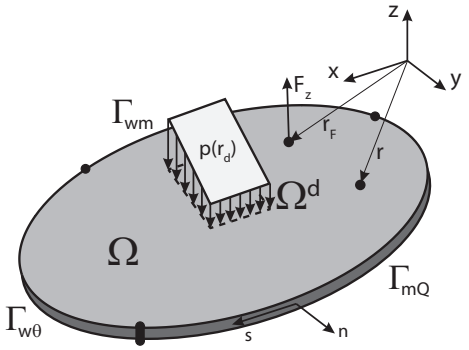

Figure 1: General plate bending problem.

The Kirchhoff equation (1), being a fourth order partial differential equation, requires two boundary conditions at every point on the problem boundary $\Gamma = \partial\Omega = \Gamma_{w\theta} \cup \Gamma_{mQ} \cup \Gamma_{wm}$. For an easy understanding, the boundary conditions which are further used in the paper, are

recapitulated. The prescribed values for the out-of-plane displacement, rotation, generalised shear force and bending moment are written as $\overline{w}_z$, $\overline{\theta}_n$, $\overline{Q}_n$ and $\overline{m}_n$, respectively. The differential operators associated with these derived quantities, $\mathcal{L}_{\theta_n}$, $\mathcal{L}_{m_n}$ and $\mathcal{L}_{Q_n}$ are defined as:

$$\mathcal{L}_{\theta_n} = -\frac{\partial}{\partial n}, \tag{4}$$

$$\mathcal{L}_{m_n} = -D\left(\frac{\partial^2}{\partial n^2} + \nu\frac{\partial^2}{\partial s^2}\right), \tag{5}$$

$$\mathcal{L}_{Q_n} = -D\frac{\partial}{\partial n}\left[\frac{\partial^2}{\partial n^2} + (2-\nu)\frac{\partial^2}{\partial s^2}\right], \tag{6}$$

with n and s the in-plane normal and tangential directions to the plate boundary Γ, as indicated in Fig. 1.

With this notation, the boundary conditions can be expressed as follows:

- Kinematic boundary conditions with prescribed values on displacements and rotations:

$$\mathbf{r} \in \Gamma_{w\theta} : \left\{ \begin{array}{rcl} R_{w_z}(\mathbf{r}) &=& w_z(\mathbf{r}) - \overline{w}_z(\mathbf{r}) \quad = \quad 0 \\ R_{\theta_n}(\mathbf{r}) &=& \mathcal{L}_{\theta_n}\left[w_z(\mathbf{r})\right] - \overline{\theta}_n(\mathbf{r}) \quad = \quad 0 \end{array} \right. . \tag{7}$$

  The clamped edge boundary condition, which is used in the validations, is a kinematic boundary condition with all displacements and rotations constrained.

- Mechanical boundary conditions with prescribed values of the stress resultants. However, since only two boundary conditions can be imposed, the shear force q_n and the twisting moment m_{ns} are combined into a generalised shear force:

$$Q_n = q_n + \frac{\partial m_{ns}}{\partial s}. \tag{8}$$

  With this generalised shear force, the mechanical boundary conditions are defined as:

$$\mathbf{r} \in \Gamma_{mQ} : \left\{ \begin{array}{rcl} R_{m_n}(\mathbf{r}) &=& \mathcal{L}_{m_n}\left[w_z(\mathbf{r})\right] - \overline{m}_n(\mathbf{r}) \quad = \quad 0 \\ R_{Q_n}(\mathbf{r}) &=& \mathcal{L}_{Q_n}\left[w_z(\mathbf{r})\right] - \overline{Q}_n(\mathbf{r}) \quad = \quad 0 \end{array} \right. . \tag{9}$$

- Mixed boundary conditions with prescribed values on displacements and bending moments:

$$\mathbf{r} \in \Gamma_{wm} : \left\{ \begin{array}{rcl} R_{w_z}(\mathbf{r}) &=& w_z(\mathbf{r}) - \overline{w}_z(\mathbf{r}) \quad = \quad 0 \\ R_{m_n}(\mathbf{r}) &=& \mathcal{L}_{m_n}\left[w_z(\mathbf{r})\right] - \overline{m}_n(\mathbf{r}) \quad = \quad 0 \end{array} \right. . \tag{10}$$

  The simply supported boundary condition, which is used in the validations, is a mixed boundary condition with constrained displacements and zero bending moments.

3. The WBM for plate bending problems

This section discusses the basic concepts of the WBM for the analysis of plate bending problems, as introduced by Desmet [21] and further developed by Vanmaele [10, 30]. Firstly, the different steps of the modelling procedure are briefly listed. Thereafter, each step is further elaborated.

3.1. Basic concept

The WBM [21] is a deterministic numerical technique for solving a set of Helmholtz equations under given boundary conditions. It follows an indirect Trefftz [11] approach, i.e. it applies exact solutions of the governing differential equations as solution expansion functions. For structural bending problems, these so-called wave functions exactly satisfy the Kirchhoff equation (1).

The modelling procedure consists of four steps:

1. Partitioning of the considered problem domain into convex subdomains.
2. Selection of the wave functions in the out-of-plane displacement expansion.
3. Construction of the WBM system matrices using a weighted residual formulation of the boundary and interface conditions.
4. Solution of the system for the unknown wave function contribution factors and postprocessing for the dynamic variables (out-of-plane displacement) and the derived dynamic variables (stresses, structural intensity, ...).

3.2. Partitioning strategy

Desmet [21] showed that convexity of the considered problem domain is a sufficient condition to ensure the convergence of the WBM. However, for many practical applications, the problem geometry may be non-convex. In that case, the problem should be divided into N_Ω number of non-overlapping, convex subdomains $\Omega^{(\beta)}$. To ensure continuity between the different subdomains, coupling conditions must be applied at the corresponding interfaces [39]. In this paper, however, only one wave based domain is considered. The concepts developed in this paper can be readily extended to non-convex problem geometries with multiple subdomains using partitioning methods as explained in [10].

3.3. Wave function selection

The steady-state out-of-plane displacement $w_z(\mathbf{r})$ is approximated by a weighted sum $\hat{w}_z(\mathbf{r})$ of n_b number of wave functions $\Psi_b(\mathbf{r})$ with their corresponding weights w_b. This sum is completed with particular solutions consisting of $\hat{w}_F(\mathbf{r})$ for a force loading and $\hat{w}_p(\mathbf{r})$ for a distributed pressure loading:

$$w_z(\mathbf{r}) \approx \hat{w}_z(\mathbf{r}) = \sum_{b=1}^{n_b} \Psi_b(\mathbf{r}) w_b + \hat{w}_F(\mathbf{r}) + \hat{w}_p(\mathbf{r}) = \mathbf{\Psi_b}(\mathbf{r})\mathbf{w_b} + \hat{w}_F(\mathbf{r}) + \hat{w}_p(\mathbf{r}), \tag{11}$$

where $\mathbf{\Psi_b}(\mathbf{r})$ represents a $(1 \times n_b)$ vector collecting the wave functions $\Psi_b(\mathbf{r})$, and $\mathbf{w_b}$ an $(n_b \times 1)$ vector combining the unknown wave function contributions w_b.

Desmet [21] proposes to use a superposition of two types of wave functions:

$$\Psi_b(\mathbf{r}) = \begin{cases} \Psi_1(\mathbf{r}) = \cos\left(k_{x1}x\right) e^{-\mathrm{j}k_{y1}y} \\ \Psi_2(\mathbf{r}) = e^{-\mathrm{j}k_{x2}x} \cos\left(k_{y2}y\right) \end{cases} . \tag{12}$$

The only requirement for these wave functions to be exact solutions of the Kirchhoff equation (1) is that the wavenumber components $k_{\bullet\star}$ satisfy the following dispersion relation, where $\star$ can represent each of the two types:

$$\left[\left(k_{x\star}\right)^2 + \left(k_{y\star}\right)^2\right]^2 = \left(k_b^s\right)^4 . \tag{13}$$

A convergent set of wave functions is obtained when the following choice is made for the wavenumbers [21]:

$$\begin{cases} (k_{x1}, k_{y1}) = \left(\dfrac{b_1\pi}{L_x}, \begin{Bmatrix} \pm\sqrt{\left(k_b^s\right)^2 - \left(\frac{b_1\pi}{L_x}\right)^2} \\ \pm\mathrm{j}\sqrt{\left(k_b^s\right)^2 + \left(\frac{b_1\pi}{L_x}\right)^2} \end{Bmatrix} \right) & b_1 = 0, 1, \ldots \\ \\ (k_{x2}, k_{y2}) = \left(\begin{Bmatrix} \pm\sqrt{\left(k_b^s\right)^2 - \left(\frac{b_2\pi}{L_y}\right)^2} \\ \pm\mathrm{j}\sqrt{\left(k_b^s\right)^2 + \left(\frac{b_2\pi}{L_y}\right)^2} \end{Bmatrix}, \dfrac{b_2\pi}{L_y} \right) & b_2 = 0, 1, \ldots \end{cases} , \tag{14}$$

where the lengths L_x and L_y are the dimensions of the preferably [21] smallest rectangle enclosing the corresponding subdomain, as shown in Fig. 2.

In order to be applied in a numerical scheme, the infinite set of wave functions needs to be truncated. The upper value of the parameters $b_\star$ in the wavenumber selection procedure (14) is

chosen according to a frequency dependent truncation rule:

$$\frac{\pi b_\star}{L_\bullet} \geq T k_b^s, \tag{15}$$

which can be interpreted as using all wave functions with a wavelength larger than or equal to $1/T$ times the physical wavelength at the studied frequency. A typical range for the truncation parameter for out-of-plane structural calculations is $1 \leq T \leq 6$ [40].

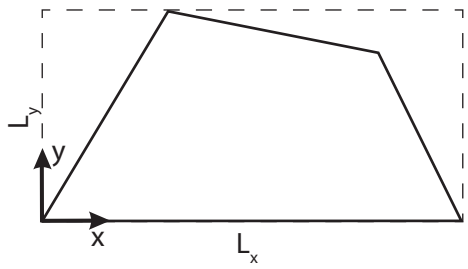

Figure 2: Circumscribing rectangle (- - - -).

This leads to a total number of bending wave functions n_b:

$$n_b = 4\left(n_{b1}+1\right) + 4\left(n_{b2}+1\right). \tag{16}$$

The expansion (11) is completed using particular solution functions $\hat{w}_F(\mathbf{r})$ and $\hat{w}_p(\mathbf{r})$. The steady-state response $\hat{w}_F(\mathbf{r})$ of an infinite homogeneous structural domain under a point force F_z is given by:

$$\hat{w}_F(\mathbf{r}) = \frac{\mathrm{j}F_z}{8\left(k_b^s\right)^2 D}\left[H_0^{(2)}\left(k_b^s d(\mathbf{r},\mathbf{r_F})\right) - H_0^{(2)}\left(-\mathrm{j}k_b^s d(\mathbf{r},\mathbf{r_F})\right)\right], \tag{17}$$

where $d(\mathbf{r},\mathbf{r_F}) = \sqrt{(x-x_F)^2+(y-y_F)^2}$ is the distance between the point $\mathbf{r_F} = (x_F, y_F)$ where the force is applied and a point at coordinates $\mathbf{r} = (x, y)$. The Hankel function of the second kind of order 0 is represented by $H_0^{(2)}$. Figure 3 shows a typical dynamic field of such a particular solution function $\hat{w}_F(\mathbf{r})$.

So far, particular solutions $\hat{w}_p(\mathbf{r})$ for distributed loads have only been briefly touched upon by Desmet [21] and Jegorovs [37]. Section 4 will discuss two different strategies to derive particular solutions for a distributed load over a plate.

3.4. Construction of the WBM model

The expansion functions (12), with the selected wavenumber components (14), ensure that the Kirchhoff equation is always satisfied, independently of the wave function contribution factors.

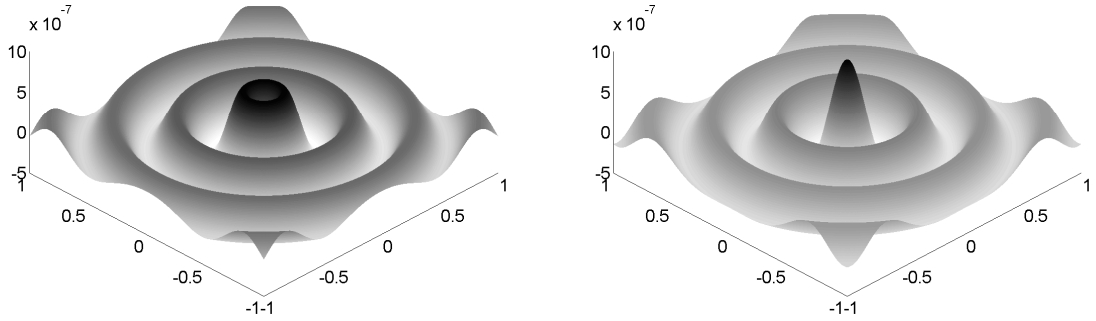

(a) Real part (b) Imaginary part

Figure 3: Particular solution $\hat{w}_F(\mathbf{r})$ with F_z=1 N at $\mathbf{r_F}$=(0,0), k_b^s=16.33 m^{-1} and D=519.2 Pa/m^3.

However, the boundary conditions may still be violated. These errors can be minimised through a weighted residual formulation:

$$\sum_i^{N_B} \int_{\Gamma_i} \tilde{t}_i(\mathbf{r}) \left(\mathcal{B}_i(\hat{w}_z(\mathbf{r})) - \overline{\mathcal{B}}_i(\mathbf{r}) \right) d\Gamma = 0, \tag{18}$$

where N_B represents the number of boundaries on which different boundary conditions are imposed, $\tilde{t}_i$ is an arbitrary weighting function for imposed boundary conditions and $\mathcal{B}_i$ is a general boundary differential operator on the boundaries with an imposed field represented by $\overline{\mathcal{B}}_i(\mathbf{r})$. The introduction of the same expansion for the field variables and weighting functions into (18) yields an algebraic system of equations, linking the contributions of the n_b number of wave functions $\Psi_b(\mathbf{r})$:

$$\mathbf{A_{bb}} \mathbf{w_b} = \mathbf{f_b}, \tag{19}$$

where $\mathbf{A_{bb}}$ represents the WBM system matrix and $\mathbf{f_b}$ the external excitation vector. The unknowns in this system of equations are the wave function contributions $\mathbf{w_b}$ which minimise the error residuals on the imposed boundaries and interfaces.

3.5. Solution of the system of equations and postprocessing

The final step in the WBM modelling procedure is the solution of the WBM system of equations (19) for the unknown wave function contributions $\mathbf{w_b}$. Back-substitution of these contribution factors into the field variable expansion (11) yields an approximation of the displacement field in

the dynamic out-of-plane vibrations. By applying the appropriate differential operators [41] to the wave function sets, derived variables (such as the stresses or structural intensity) can be calculated with the same spatial resolution, unlike with the element-based methods with their polynomial shape functions.

4. Particular solution functions for distributed pressure loads

This section discusses the development of two particular solutions for the WBM when a distributed pressure load normal to the plate is applied.

The first approach is based on the integration of point force particular solutions. This approach explicitly calculates the response of an infinite plate by integrating the applied pressure profile over the patch surface. The wave functions are then weighted in such a way that the total field, i.e. particular solution and wave function expansion, satisfies the applied boundary conditions.

The second approach addresses the problem from a different perspective. Using the Fourier transformation, the applied pressure profile is decomposed into a number of plane waves. For each of these plane waves, the Kirchhoff equation is solved. Each component of this second particular solution set can thus be seen as the response of a rectangular plate to an incoming plane wave. Again, the weighting of the wave functions makes sure that the total field satisfies the applied boundary conditions.

The section is concluded with a short summary of the properties of both particular solution sets.

4.1. Hankel-based approach – Integration of point forces

In this first approach, a particular solution function is developed based on the deformation of an infinite homogeneous plate under a point force (17). By considering a pressure field p as an infinite sum of discrete point forces, the expression for the particular solution $\hat{w}_p(\mathbf{r})$ can be seen as an infinite sum over the particular solution to these discrete point forces. This gives the following expression:

$$\hat{w}_p(\mathbf{r}) = -\frac{\mathrm{j}}{8\left(k_b^s\right)^2 D}\int_{\Omega^d} p(\mathbf{r_d})\left[H_0^{(2)}\left(k_b^s d(\mathbf{r},\mathbf{r_d})\right) - H_0^{(2)}\left(-\mathrm{j}k_b^s d(\mathbf{r},\mathbf{r_d})\right)\right] d\Omega^d. \tag{20}$$

Application of the appropriate differential operators (4)-(6) gives similar expressions for derived quantities $\hat{\theta}_{n,p}(\mathbf{r})$, $\hat{m}_{n,p}(\mathbf{r})$ and $\hat{Q}_{n,p}(\mathbf{r})$, which are functions with the same spatial resolution as $\hat{w}_p(\mathbf{r})$.

However, the calculation of these functions is relatively expensive, since for every evaluation at $\mathbf{r}$, a surface integral has to be calculated over Ω^d. Moreover, due to the highly oscillatory nature of these particular solutions (see Fig. 3), care has to be taken in the evaluation of this surface integral.

In order to do so, a Gauss-Legendre integration scheme [45], using a specified number of points per physical wavelength is used. This can, however, limit the accuracy since the distributed pressure $p(\mathbf{r})$ is discretised in the Gauss points. In a convergence study, as further illustrated, this can lead to a stagnation of the solution to the accuracy of the pressure field approximation. To overcome this, the number of Gauss points can be increased using a numerical integration parameter T_H:

$$T_H = \frac{n_{gp,Hankel}}{n_{gp,WF,T=1}}, \tag{21}$$

where $n_{gp,Hankel}$ indicates the number of Gauss points per wavelength used for the integration of the particular solutions and $n_{gp,WF,T=1}$ the number of Gauss points per wavelength for the integration of the wave functions for a wave function truncation of $T = 1$. For load profiles of moderate complexity, however, $T_H = 1$ gives a sufficient prediction accuracy.

4.2. Fourier-based approach – Decomposition in the wavenumber domain

Since the imposed pressure field can be decomposed into a number of plane waves, alternative expressions for the particular solution function $\hat{w}_p(\mathbf{r})$ can be found, avoiding expensive surface integrals of highly oscillatory Hankel-functions. This alternative method to compute particular solution functions was briefly touched by Desmet [21] and Jegorovs [37]. By application of the Fourier transformation, the Kirchhoff equation (1) can be solved in the wavenumber domain. The particular solution in the spatial domain can then be calculated by an inverse Fourier transformation.

Firstly, the theoretical aspects of this approach are illustrated. Thereafter, the numerical procedure, including sampling and truncation, is elaborated.

4.2.1. Theoretical procedure

With the definition of the Fourier transformation $G(k_x, k_y)$ of a function $g(x, y)$ [42]:

$$G(k_x, k_y) = \int_{-\infty}^{\infty} \int_{-\infty}^{\infty} g(x, y) e^{-\mathrm{j}(k_x x + k_y y)} dx dy, \tag{22}$$

and the Kirchhoff equation (1) in the wavenumber domain (without a point force F_z):

$$\left[\left((k_x)^2 + (k_y)^2 \right)^2 - (k_b^s)^4 \right] W(k_x, k_y) = -\frac{P(k_x, k_y)}{D}, \tag{23}$$

$W(k_x, k_y)$, the solution in the wavenumber domain (k_x, k_y) of an infinite plate under a distributed load can be found:

$$W(k_x, k_y) = -\frac{P(k_x, k_y)}{D\left[\left((k_x)^2 + (k_y)^2\right)^2 - \left(k_b^s\right)^4\right]}. \tag{24}$$

Using the inverse Fourier transformation, defined as:

$$g(x, y) = \frac{1}{(2\pi)^2} \int_{-\infty}^{\infty} \int_{-\infty}^{\infty} G(k_x, k_y) e^{\mathrm{j}(k_x x + k_y y)} dk_x dk_y, \tag{25}$$

the solution is obtained in the spatial domain (x, y). This function satisfies the Kirchhoff equation with a distributed load and can thus be used as a particular solution. Combining (22)-(25), the general expression for the particular solution function $\hat{w}_p(\mathbf{r})$ thus becomes:

$$\hat{w}_p(\mathbf{r}) = -\frac{1}{(2\pi)^2} \int_{-\infty}^{\infty} \int_{-\infty}^{\infty} \frac{\int_{-\infty}^{\infty} \int_{-\infty}^{\infty} p(\mathbf{r}) e^{-\mathrm{j}(k_x x + k_y y)} dx dy}{D\left[\left((k_x)^2 + (k_y)^2\right)^2 - \left(k_b^s\right)^4\right]} e^{\mathrm{j}(k_x x + k_y y)} dk_x dk_y. \tag{26}$$

For a harmonic pressure excitation $p(\mathbf{r})$, the analytical expression for $\hat{w}_p(\mathbf{r})$ (26) can be simplified. With the transformation pairs for sines and cosines,

$$g(r) = \sin(k_r r) \leftrightarrow G(k_r) = \frac{\pi}{\mathrm{j}} \left(\delta(k - k_r) - \delta(k + k_r)\right), \tag{27}$$

$$g(r) = \cos(k_r r) \leftrightarrow G(k_r) = \pi \left(\delta(k - k_r) + \delta(k + k_r)\right), \tag{28}$$

and using the multiplication-convolution theorem,

$$g(r)h(s) \leftrightarrow G(k_r) * H(k_s), \tag{29}$$

the forward and inverse transformations can be done analytically. In this case, (26) simplifies to

$$\hat{w}_p(\mathbf{r}) = -\frac{p(\mathbf{r})}{D\left[\left((k_x)^2 + (k_y)^2\right)^2 - \left(k_b^s\right)^4\right]}. \tag{30}$$

Note also that a uniform excitation can be considered as a harmonic cosine-cosine function with $(k_x, k_y) = (0, 0)$.

4.2.2. Numerical procedure

For pressure fields with a non-harmonic spatial variation of the distributed load, (26) cannot be calculated analytically. A discretised Fourier transformation is necessary and requires a choice for the sampling rate and the truncation, both in the wavenumber domain and the spatial domain.

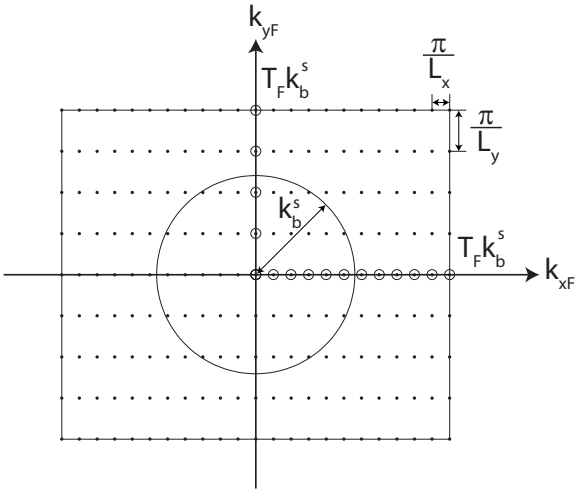

Figure 4: Choice of the Fourier projection functions $\bullet_F$ and their relation to the WBM function set with $\circ$ indicating the chosen wave function components (14) and $\cdot$ indicating the chosen projection function components (31).

Since the particular solution expansion will strongly interact with the wave function expansion, it is logical to choose the wavenumber selection and truncation in an analogical manner. For the wavenumber domain sampling, this means that functions are chosen such that a half wavelength fits into the circumscribing rectangle:

$$(k_{xF}, k_{yF}) = \left(\frac{b_1 \pi}{L_x}, \frac{b_2 \pi}{L_y} \right), \tag{31}$$

with b_1 and b_2 defined in (14) and the subscript $\bullet_F$ indicating the discretised wavenumber.

A similar frequency dependent truncation rule as in (15) applies, such that only projection functions with a wavelength larger than or equal to $1/T_F$ times the physical wavelength are used, with T_F the wavenumber domain truncation parameter. Because of the resemblance with the wave functions, $T_F = T$ is used as a standard setting. Fig. 4 shows this transition from an infinite, continuous wavenumber domain into a truncated and discretely sampled domain.

Also in the spatial domain, truncation and sampling are necessary. Since the actual plate under study is finite, it is not necessary to perform the integration in (22) outside the plate domain. Moreover, as the wavenumbers are defined on the rectangle enclosing the domain, the spatial truncation boundaries are set to be coincident with that rectangle.

The spatial sampling periods Δ_{Nyq} are directly related to the wavenumber truncation $T_F k_b^s$.

The relation between both is given by the Shannon-Nyquist sampling theorem [43]:

$$\Delta_{Nyq} \leq \frac{\pi}{T_F k_b^s}. \tag{32}$$

The maximal values allowed by (32) are used.

4.3. Summary

As a short conclusion to this section, the main advantages and disadvantages of the two particular solution function sets are summarised here.

Decomposition. The Hankel based approach approximates the particular solution field as a superposition of point force particular solutions; it uses a spatial decomposition of the load. The Fourier-based approach approximates the pressure excitation field through a three-step procedure involving a forward and an inverse Fourier transformation. Between both Fourier-based steps, a particular solution function is calculated for each Fourier component by solving the Kirchhoff equation in the wavenumber domain. This approach thus utilises a spectral decomposition.

Discretisation. In order to discretise the the Hankel based approach, number of point forces can be controlled through a parameter T_H, which can be interpeted as using T_H times the number of Gauss points used per wavelength for the numerical integration of the wave functions. The standard setting is $T_H = 1$. The continuous Fourier transformation has to be both discretised and sampled, both in the wavenumber domain and in space. In the wavenumber domain, the same choices as for the wave functions are made in terms of sampling and truncation $T_F = T$. In the spatial domain, the domain bounding box is used for truncation and the Nyquist theorem is applied for the sampling.

Interpretation. The Hankel based solution set describes in essence the response of an infinite plate under a loaded patch. In the Fourier-based approach, each of the particular solutions can be interpreted as the response of an infinite plate to an incoming plane wave.

Applicability. Since the computational cost for the point force approximation functions in the Hankel-based approach is proportional to the surface of the loaded patch, it shows to be most useful in the field of small, localised patches or spatially complex (non-harmonic) loads. As the

second approach makes intensively use of the Fourier transformation, it will perform best for harmonic and harmonically decomposable distributed loads. For smaller surfaces, Gibbs phenomena will impede a high accuracy.

5. Numerical validation

This section evaluates the performance of the distributed load strategies for the WBM for structural bending problems by means of two numerical validations with increasing complexity. The first problem case considers a square plate, for which an analytical solution is available. The second problem case considers a quadrilateral plate. For both problem settings, four different load cases are considered. Two different materials are used, of which the properties are given in Tab. 1.

	Material 1: Steel	Material 2: Aluminium
Elasticity modulus	E=210·10^{9}Pa	E=70·10^{9}Pa
Material loss factor	$\eta = 0$	$\eta = 0.01$
Poisson ratio	$\nu = 0.3$	$\nu = 0.3$
Material density	ρ=7800kg/m^3	ρ=2790kg/m^3

Table 1: Material properties used in the numerical validation.

Results obtained with the WBM are compared to results obtained with the Rayleigh-Ritz [44] method and with the FEM. The comparisons are made in terms of calculation times and accuracy. Ansys 12.1 is used for the FEM reference models. The WBM routines are implemented in Matlab R2010a. All calculations are performed on a Windows-based 2.52 GHz Intel Xeon system with 32 GB RAM.

5.1. Validation case 1

The first validation case considers a square (1m × 1m) steel plate (Tab. 1) as shown in Figure 5(a) with $t = 3$mm thickness. The plate is simply supported on all four edges. Four different load cases (Fig. 5(b) to 5(e)) are chosen such that there is a gradual increase from a highly localised patch load to a global harmonic load, in order to show the strengths and weaknesses of the two particular solutions: those based on the integration of Hankel-based particular solutions for a point force and those based on a decomposition of the distributed load in the wavenumber domain, respectively.

For all configurations, the out-of-plane structural displacement $w_z(\mathbf{r})$ is shown at a frequency of 700 Hz (Fig. 6 to 9). Below this frequency, the plate has 60 modes. This clearly indicates its

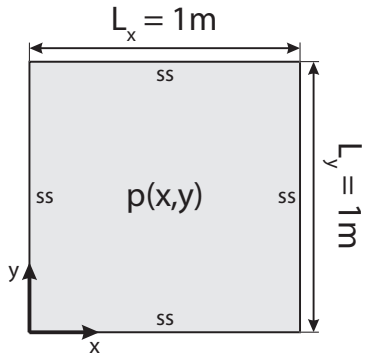

(a) Square plate with simply supported (ss) boundary conditions.

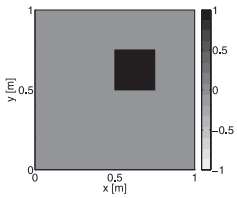

(b) Load case 1 – $p(\mathbf{r_d}) = 1$ Pa with $\mathbf{r_d} \in [0.50, 0.70] \cup [0.50, 0.70]$; (cfr. λ_b=0.206 m)

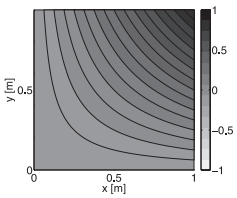

(c) Load case 2 – $p(\mathbf{r}) = x \cdot y$ Pa.

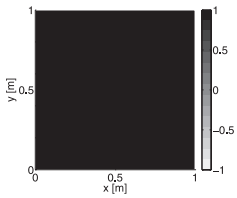

(d) Load case 3 – $p(\mathbf{r}) = 1$ Pa.

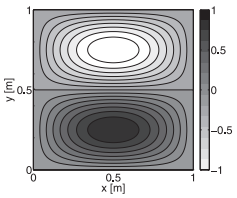

(e) Load case 4 – $p(\mathbf{r}) = \sin(\pi x)\sin(2\pi y)$ Pa.

Figure 5: Problem geometry and applied load cases for Case 1.

mid- to high-frequency behaviour. The calculations are made with a truncation setting $T = 4$, resulting in 312 wave functions. Both approaches are used in their standard setting, as discussed in Section 4; the Hankel-based approach is used with the numerical integration setting $T_H = 1$ and the Fourier-based approach is used with the truncation setting $T_F = T$.

The results are compared to the analytical solution obtained with the Rayleigh-Ritz method, using 40000 modes. Details on the derivation of the analytical solution are given in Appendix A.

To assess the accuracy, logarithmic error contour plots relative to the analytical solution are shown. This relative prediction error $\varepsilon(\mathbf{r})$ is defined as:

$$\varepsilon(\mathbf{r}) = \left| \frac{w_z^{\bullet}(\mathbf{r}) - w_z^{ref}(\mathbf{r})}{w_z^{ref}(\mathbf{r})} \right|, \tag{33}$$

where $\bullet$ represents the result obtained with the WBM with either the Hankel- or the Fourier-based

particular solutions and $w_z^{ref}(\mathbf{r})$ represents the Rayleigh-Ritz reference solution.

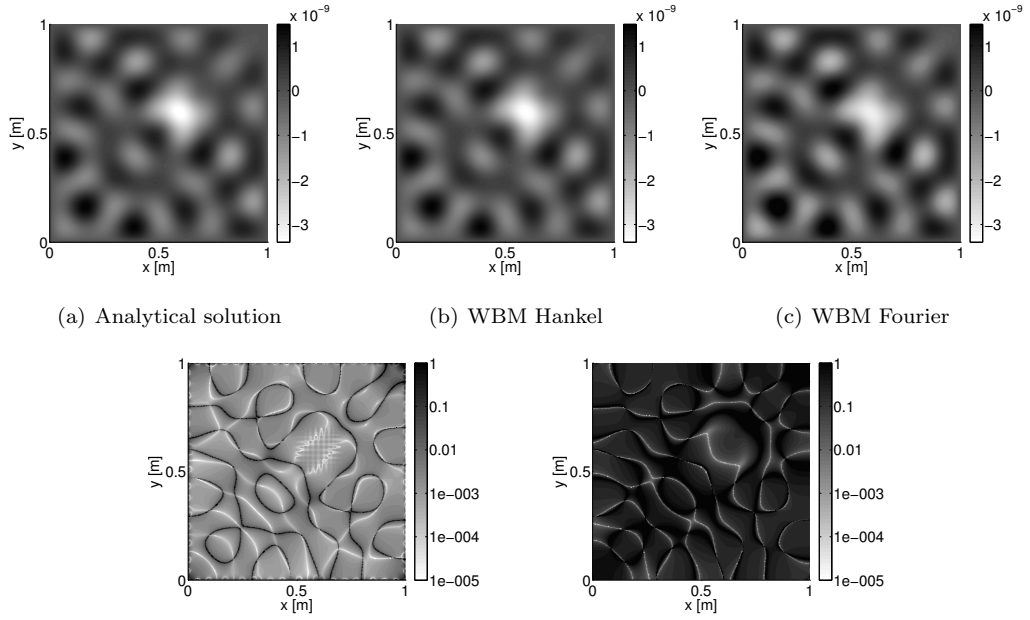

(a) Analytical solution (b) WBM Hankel (c) WBM Fourier

(d) Error WBM Hankel (e) Error WBM Fourier

Figure 6: Out-of-plane deformation $w_z(\mathbf{r})$: Amplitude [m] and relative prediction error ε [-] at 700 Hz for Load case 1.

For Load case 1, Fig. 6(a) to 6(c) are very similar, illustrating the applicability of both particular solution approaches. However, the error contour plot for the Hankel-based functions (Fig. 6(d)) shows that the overall accuracy is much higher than for the Fourier-based functions (Fig. 6(e)). The Hankel-based approach accounts for an accuracy in the order of 1%, which is a very good accuracy, especially relative to the effect of variability in this frequency range. The error using the Fourier-based functions, however is up to 100%. Also note that the higher error at the nodal lines results from an inaccurate error calculation due to almost-zero division.

This difference in accuracy can be readily explained by how the two approaches deal with discontinuities. The Hankel-based functions (20) are defined by an integration over the loaded surface Ω^d. For a patch load, the discontinuity at the edges of this patch induces Gibbs phenomena for the Fourier-based approach, whereas it only confines the integration domain Ω^d in the Hankel-approach without further problem.

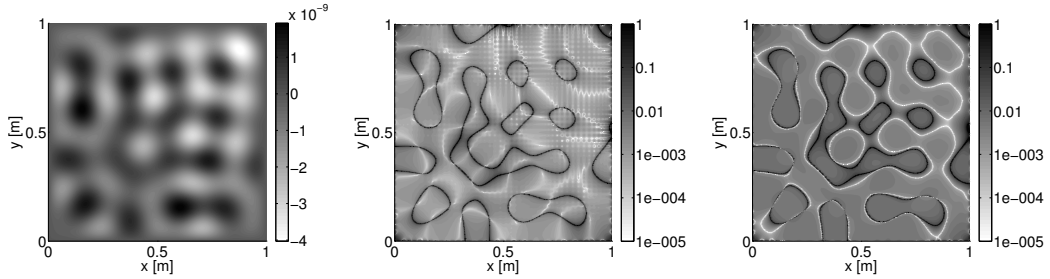

(a) Analytical solution (b) Error WBM Hankel (c) Error WBM Fourier

Figure 7: Out-of-plane deformation $w_z(\mathbf{r})$: Amplitude [m] and relative prediction error ε [-] at 700 Hz for Load case 2.

For the globally defined distributed load in Load case 2 (Fig. 7(a)), the error levels for both approaches are closer to each other (Fig. 7(b)-7(c)). Now the projection functions in the Fourier-based particular solutions no longer have to deal with a sharp discontinuity inside the problem domain, giving an accuracy in the order of 5%. Therefore, the pressure decomposition is more accurate than the previous one. However, also for this application, the Hankel-based approach is more accurate. The accuracy is still in the order of 1%, as can be expected; the fine integration can account for any pressure distribution.

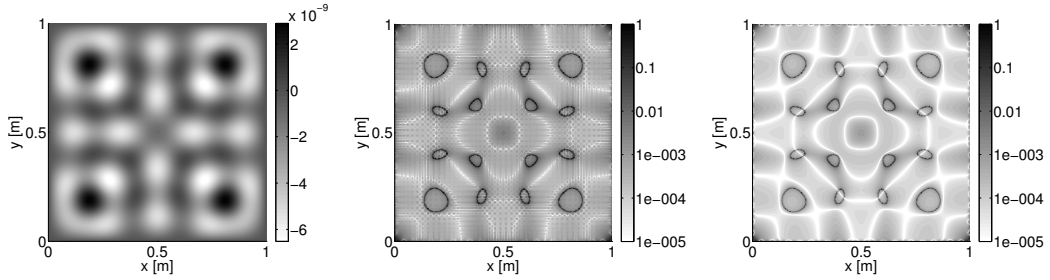

(a) Analytical solution (b) Error WBM Hankel (c) Error WBM Fourier

Figure 8: Out-of-plane deformation $w_z(\mathbf{r})$: Amplitude [m] and relative prediction error ε [-] at 700 Hz for Load case 3.

Logically, the Fourier-based approach is at its best when the forward and inverse Fourier transformation can be done analytically (30), as is the case for harmonic loading. For Load case 3, which is a uniform load (Fig. 8), the accuracy of the Fourier-based functions (Fig. 8(c)) strongly improves

to 0.5% since the calculation of the particular solution can be done exactly. The accuracy of the Hankel-based approach (Fig. 8(b)) again is in the order of 1%, very similarly to Load case 1 and 2.

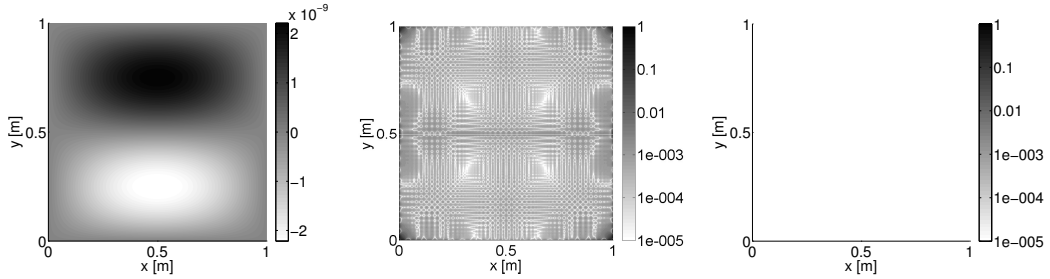

(a) Analytical solution (b) Error WBM Hankel (c) Error WBM Fourier

Figure 9: Out-of-plane deformation $w_z(\mathbf{r})$: Amplitude [m] and relative prediction error ε [-] at 700 Hz for Load case 4.

The results of Load case 4 (Fig. 9) are trivial. The solution for the Fourier-based approach (Fig. 9(c)) is exact, as the particular solution is also the analytical solution for this configuration. Therefore, all wave functions coming from the homogeneous part of the solution have zero contributions and no approximation error whatsoever is made.

5.2. Validation case 2

The second validation case considers a quadrilateral (1m $\times$ 0.5m) aluminium plate (Tab. 1) as shown in Figure 10(a) with a $t = 2$mm thickness . The plate is clamped on all four edges. Again, four different load cases (Fig. 10(b)-10(e)) are applied.

In a first validation of this problem case, the convergence of the developed particular solutions is studied and compared to FEM reference models. To avoid averaging out possible outliers, a global quadratic error estimator $< \delta >$ over n number of points is defined analogously to (33):

$$< \delta >= \sqrt{\frac{\sum_{i=1}^{n} \left| w_z^{\bullet}(\mathbf{r_i})^2 - w_z^{ref}(\mathbf{r_i})^2 \right|}{\sum_{i=1}^{n} \left| w_z^{ref}(\mathbf{r_i})^2 \right|}}. \tag{34}$$

This quadratic error estimator $< \delta >$ is plotted as a function of the CPU time. This CPU time is composed of the time required for the frequency-dependent operations. This means that for the FEM, the system building is not included, only the solving. For the WBM, however, the system

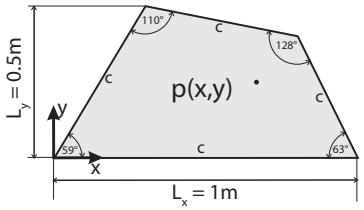

(a) Quadrilateral plate with clamped (c) boundary conditions.

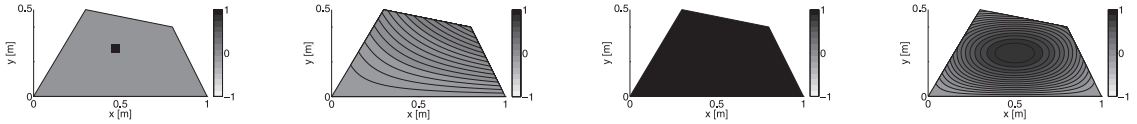

(b) Load case 1 – $p(\mathbf{r_d}) = 1$ Pa with $\mathbf{r_d} \in [0.45, 0.50] \cup [0.25, 0.30]$.

(c) Load case 2 – $p(\mathbf{r}) = x \cdot y$ Pa.

(d) Load case 3 – $p(\mathbf{r}) = 1$ Pa.

(e) Load case 4 – $p(\mathbf{r}) = \sin(\pi x)\sin(2\pi y)$ Pa.

Figure 10: Problem geometry and applied load cases for Case 2.

building has to be repeated at every frequency. Therefore, both system building and system solving time are included.

For the calculation of $< \delta >$, the out-of-plane displacement results at 500 Hz in $n = 384$ uniformly distributed points, matching with the nodes in the coarsest FE model, are used. The model properties for all FE and WB models are listed in Table 2 and 3. Below 500 Hz, the plate has 18 modes, indicating that this frequency is in the mid-frequency range.

When comparing the convergence behaviour of the WBM with the two types of particular solutions for the various load cases shown (Fig. 11), relative to the FEM, the advantage of the WBM and the newly developed particular solution functions is clear. However, in this comparison, a stagnation of the WBM results to the accuracy of the FEM reference is apparent. This stagnation occurs because the accuracy of the reference model is lower than the WB models with high truncation settings. Indeed, if a refined WBM reference is used, all WB models converge further (Fig. 12). Hence, in a similar manner with the plate bending problems tackled before [10, 30], also for plate bending problems with a distributed load, the WBM convergence is superior to the FEM such that a higher accuracy can be obtained with a lower computational effort.

These convergence curves confirm the observations made in the first problem case. The Fourier-

Model name	h_{max} $[m]$	Degrees of freedom 4-noded elements
K1	0.0500000	2304
K2	0.0250000	8742
K3	0.0125000	34038
K4	0.0062500	134310
K5	0.0031250	533574
Reference	0.0015625	2126982

Table 2: Properties for the FE models.

T	1	1.5	2	2.5	3	3.5	4	4.5	5	Reference
Wave functions	48	72	96	120	144	168	192	216	240	264

Table 3: Properties for the WB models.

based approach is at its best when the Fourier transformation can be done analytically, as is the case for Load case 3 with a uniform load (Fig. 12(c)) and for Load case 4 with a harmonic load (Fig. 12(d)). For more geometrically varying distributed loads (Fig. 12(b)), it converges much more slowly; due to the highly local and discontinuous patch load in Load case 1 (Fig. 12(a)), the convergence is almost stopped. The Hankel-based approach converges equally well for all four cases. The only difference is on the timings, as Load case 1 involves a much smaller loaded surface than the other cases.

When comparing the CPU times between the Fourier- and Hankel-based functions, however, the advantage of the Fourier-based functions is clear. Even for Load case 2, a non-harmonic global load case (Fig. 12(b)), the cost of performing a forward and inverse Fourier transformation is much lower than performing the expensive numerical integration over the plate surface for every point evaluation of the particular solution. As the locally loaded patch becomes smaller (Fig. 12(a)), the Hankel-based functions overtake the convergence of the Fourier-based functions and become the most appropriate strategy.

Up to this point, both function sets have been used in their standard setting, i.e. $T_F = T$ for the Fourier-based functions and $T_H = 1$ for the Hankel-based functions. Figure 13 shows

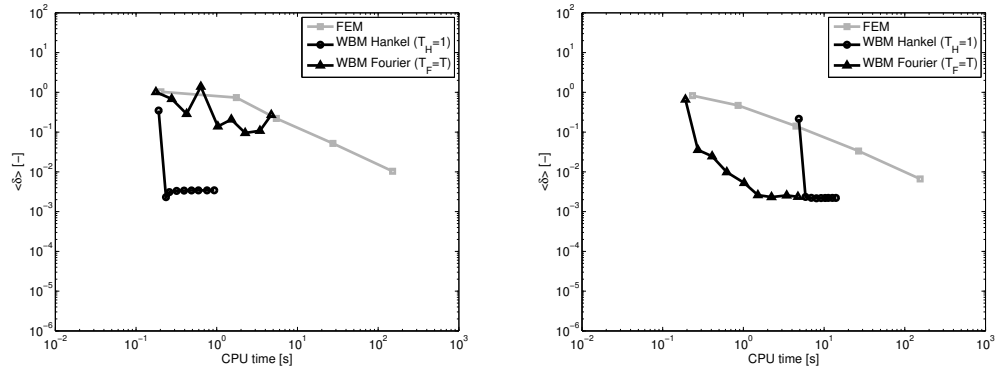

(a) Load case 1

(b) Load case 2

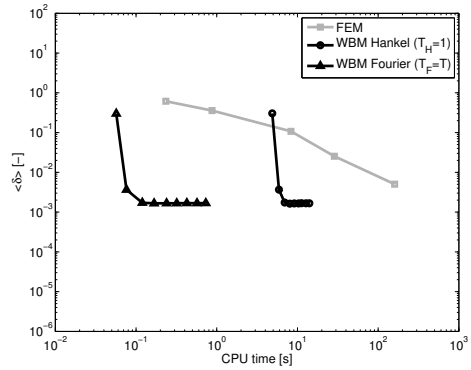

(c) Load case 3

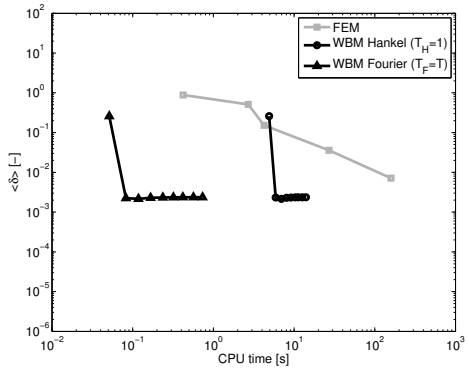

(d) Load case 4

Figure 11: Out-of-plane deformation $w_z(\mathbf{r})$: Relative prediction error δ [-] as a function of CPU time at 500 Hz (FEM reference).

the convergence curves for Load case 2 with different settings for T_F and T_H. The Fourier-based functions (Fig. 13(a)) quickly stagnates on the accuracy of the decomposition of the applied load, such that refinement of T independently of T_F makes no sense. The convergence of the Fourier-based approach is mostly governed by the distributed load decomposition and T_F. Therefore, the standard setting is chosen as $T_F = T$. The Hankel-based functions (Fig. 13(b)) are more independent of T since a setting of $T_H = 1$, for not too spatially varying loads, produces results of good accuracy. The convergence of the Hankel-based approach is mostly governed by the wave function expansion and their truncation T. Therefore, the standard setting is chosen as $T_H = 1$. If this causes a stagnation of the results, a higher value is necessary. However, choosing $T_H = T$, as is done for the

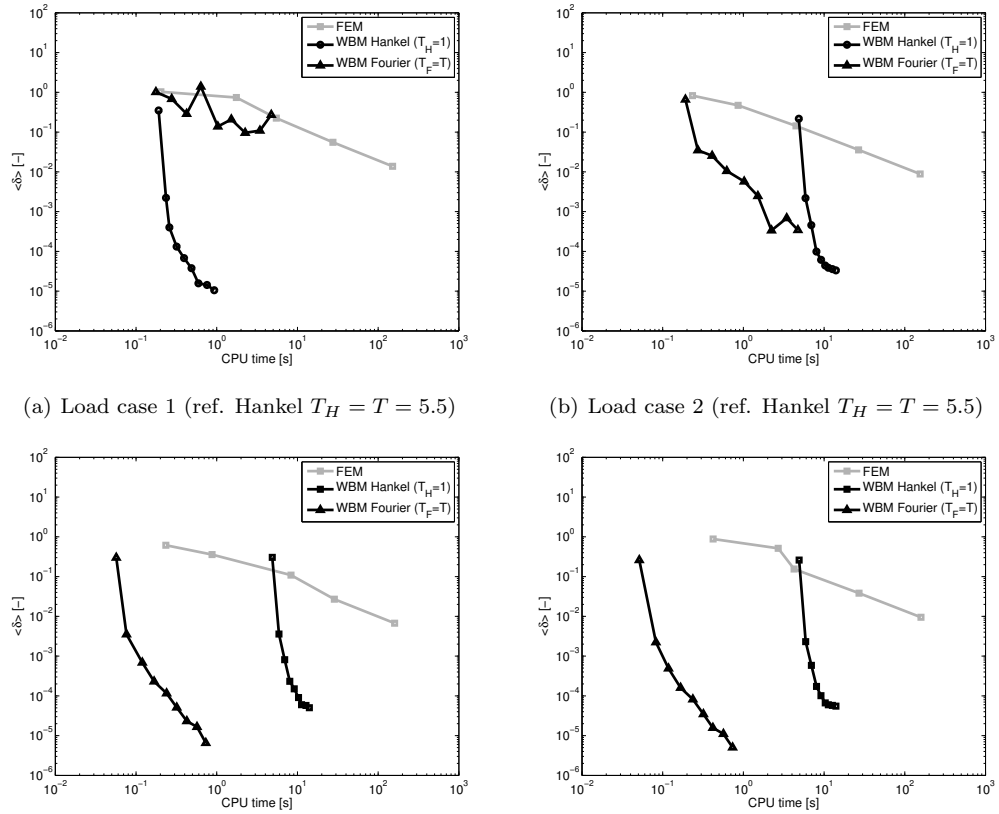

(a) Load case 1 (ref. Hankel $T_H = T = 5.5$)

(b) Load case 2 (ref. Hankel $T_H = T = 5.5$)

(c) Load case 3 (ref. Fourier $T_F = T = 5.5$)

(d) Load case 4 (ref. Fourier $T_F = T = 5.5$)

Figure 12: Out-of-plane deformation $w_z(\mathbf{r})$: Relative prediction error δ [-] as a function of CPU time at 500 Hz (WBM reference).

Fourier-based functions, is clearly too excessive. Figure 13 thus confirms that the chosen standard settings are appropriate.

The last validation considers the frequency response of the out-of-plane displacement in a response point (0.6705,0.25), indicated by • in Fig. 10(a) over the frequency band 50-1000 Hz. Two load cases are considered, both with their best performing functions: Load case 1, where the result is shown for the Hankel-based functions and Load case 3, where the result is shown for the Fourier-based functions. The WBM curves are obtained with a truncation factor of $T = 2$, using 48 wave functions at 50 Hz to 176 wave functions at 1000 Hz, and with the standard settings for T_F and T_H. The results are compared to the FE model K1 with 2304 degrees of freedom and the FEM

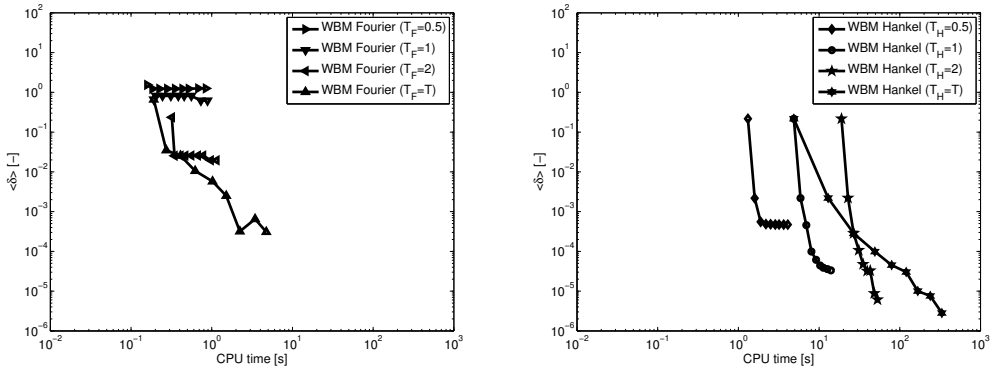

(a) Fourier (b) Hankel

Figure 13: Out-of-plane deformation $w_z(\mathbf{r})$ for Load case 2: Relative prediction error δ [-] as a function of CPU time at 500 Hz (WBM Hankel $T_H = T = 5.5$ reference).

reference solution K4 with 134310 degrees of freedom.

Figure 14(a) (Load case 1) and Figure 15(a) (Load case 3) show that over a broad frequency band, the WBM provides a good prediction accuracy at a low computational cost. Moreover, when plotting the relative error for an FEM and a WBM model with comparable timing (0.21s per frequency line for the FEM, 0.23s for the WBM with the Hankel-based particular solutions and 0.14s for the WBM with Fourier-based particular solutions), the WBM shows more accurate results, whereas the results for FE model K1 are largely influenced by numerical pollution [3, 4]. For the frequency band of 300-1000 Hz, the benchmark WBM model with $T = 2$ even outperforms the FEM reference model K4. The apparent accuracy of the WBM in Fig. 14(b) and Fig. 15(b) is actually that of the FE model K4. This is illustrated by Fig. 14(c) and Fig. 15(c), where the accuracy of the FE model K4 is shown relative to a WBM reference using a truncation of $T = 4$. These figures show that the WB models with $T = 2$ are indeed more accurate than the FE model K4.

6. Application: Turbulent Boundary Layer excitation

After the numerical validation of the newly developed particular solutions in Sec. 5, where the advantages of both approaches are demonstrated, in terms of accuracy and efficiency, a final application is studied: a plate excited by a Turbulent Boundary Layer (TBL), i.e. a distributed

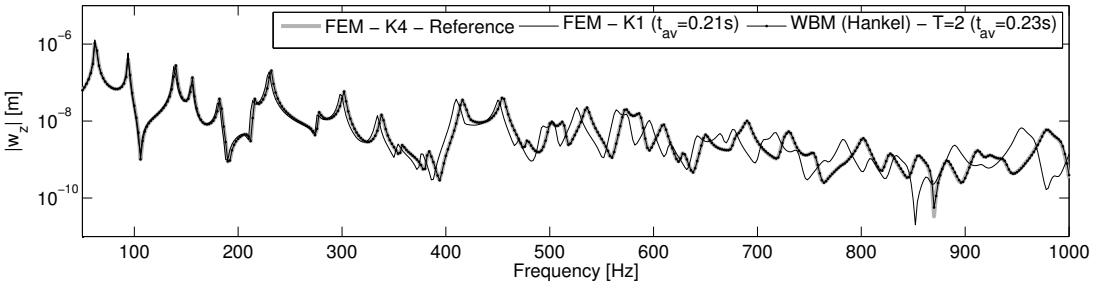

(a) FRF

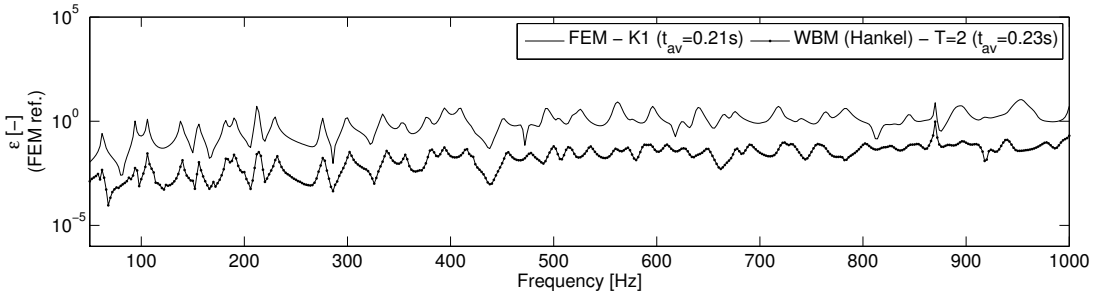

(b) Error FRF (ref. FEM)

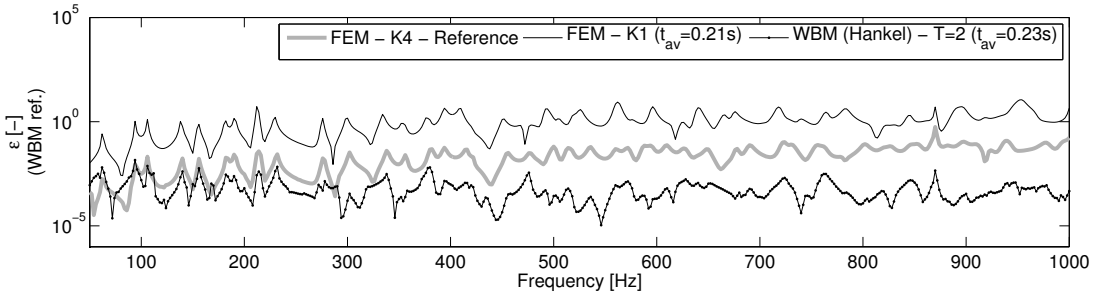

(c) Error FRF (ref. WBM)

Figure 14: Out-of-plane deformation $w_z(\mathbf{r})$ and relative error ε for a response point at (0.6705,0.25) from 50 Hz to 1000 Hz for Load case 1.

random excitation.

6.1. Corcos TBL model

The TBL wall pressure fluctuations are modelled using the empirical Corcos formulation [32]. Assuming a flow in the x-direction, the cross-spectral density S_{pp} in the space-frequency domain of

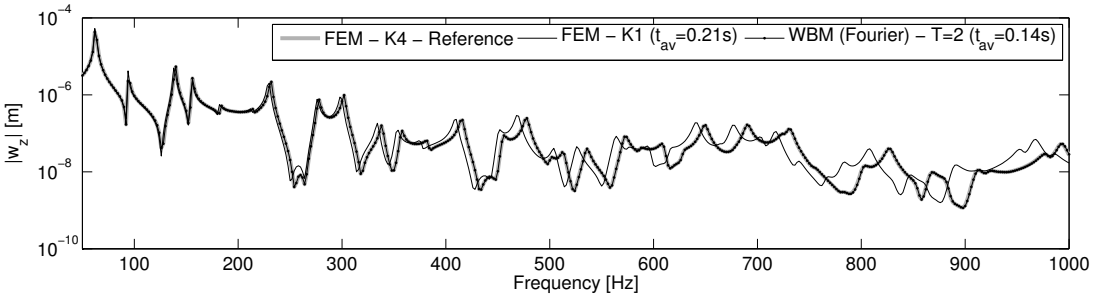

(a) FRF

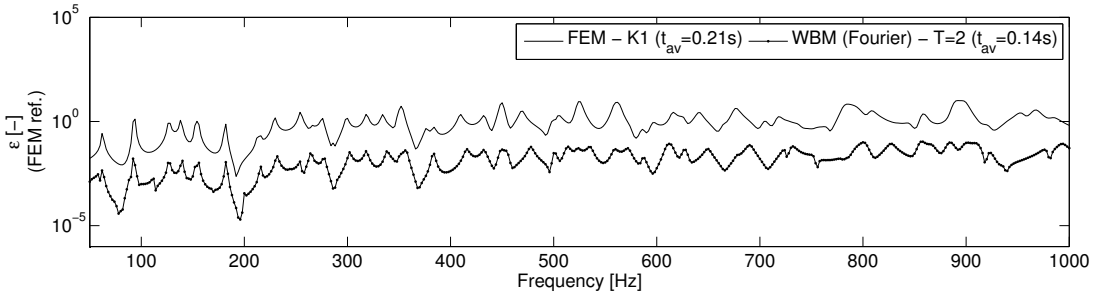

(b) Error FRF (ref. FEM)

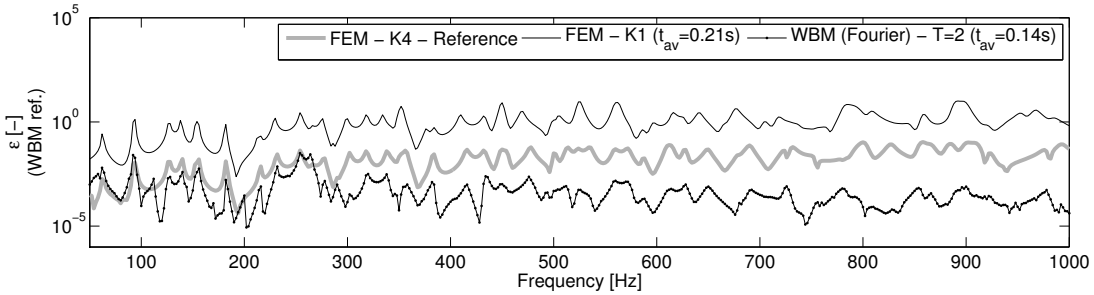

(c) Error FRF (ref. WBM)

Figure 15: Out-of-plane deformation $w_z(\mathbf{r})$ and relative error ε for a response point at (0.6705,0.25) from 50 Hz to 1000 Hz for Load case 3.

the pressure p is given by:

$$S_{pp}(\mathbf{r},\omega) = A(\omega)e^{-\alpha k_c|x|}e^{-\beta k_c|y|}e^{\mathrm{j}k_c x}, \tag{35}$$

where $k_c = \omega/U_c$ represents the convection wavenumber at the main convection velocity U_c, $A(\omega)$ is a frequency dependent amplitude and α and β are the longitudinal and lateral decay rates of

the correlation, usually determined by a curve-fit on experimental data. From this expression, the wavenumber spectrum S_{PP} can be calculated analytically:

$$S_{PP}(k_x, k_y, \omega) = \frac{A(\omega)}{k_c^2} \frac{4\alpha\beta}{\left(\alpha^2 + (1 - \frac{k_x}{k_c})^2\right)\left(\beta^2 + \left(\frac{k_y}{k_c}\right)^2\right)}. \tag{36}$$

Fig. 16 shows the spectral content of a TBL pressure field at 250 Hz.

6.2. Application in the WBM

Because of the elegant spectral form of the Corcos model (36), the Fourier based approach is best suited to tackle this problem with the WBM. Therefore, the wavenumber spectrum should again be discretised and converted into particular solutions to the Kirchhoff equation. For this, the procedure for sampling and truncation as discussed in Sec. 4.2.2, is followed. Fig. 16 shows an example of the truncation and discretisation points (•).

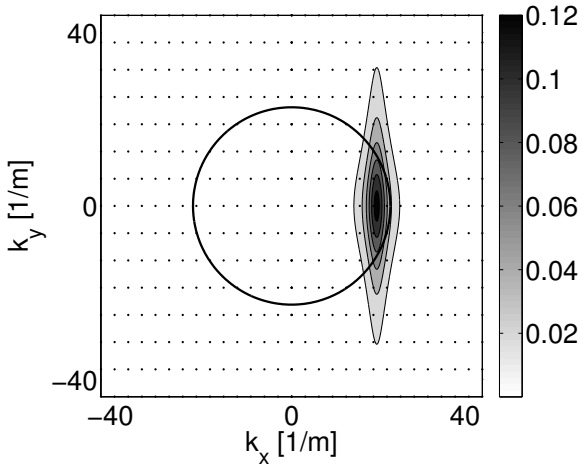

Figure 16: Absolute value of the wavenumber spectrum S_{PP} of a Corcos pressure field ($\alpha = 0.116$, $\beta = 0.7$, $U_c = 80$ m/s and $A(\omega) = 1$), $k = k_b$-circle of a 2 mm thick aluminium plate (—) and discretised wavenumber spectrum of the plane wave decomposition (•) at 250 Hz.

The plate response, in the form of the cross-spectral density S_{vv} of the out-of-plane deformation velocity, can be (numerically) calculated from:

$$\begin{aligned} S_{vv}(\mathbf{r}, \omega) &= \frac{1}{4\pi^2} \int_{-\infty}^{\infty} \int_{-\infty}^{\infty} S_{PP}(k_x, k_y, \omega) \left|H_v(\mathbf{r}, k_x, k_y, \omega)\right|^2 dk_x dk_y \\ &= \frac{1}{4\pi^2} \sum_n \sum_m S_{PP}(k_n, k_m, \omega) \left|H_v(\mathbf{r}, k_n, k_m, \omega)\right|^2 \Delta k_x \Delta k_y \end{aligned}. \tag{37}$$

This shows that the deformation velocity cross-spectral density S_{vv} can be obtained from a post-processing step on the velocity transfer functions H_v in the point $\mathbf{r}$ in response to each of the discretised uncorrelated plane waves (k_n, k_m) [46].

These velocity transfer functions H_v can be calculated very efficiently with the WBM. The method has three important advantages, as compared to traditional element-based methods. Firstly, the WBM has a low computational cost, relative to the FEM, when it comes to a dynamic plate bending problem with a distributed load. This was illustrated in Sec. 5. Secondly, earlier research [40] showed that the relative cost of multiple right hand sides is lower in the WBM as compared to the traditional element-based methods. This is because the main computational effort is in the building of the system matrices, not in their solution. Thirdly, there is no additional approximation error made in the application of the distributed harmonic load. In the WBM, particular solution functions with the same spatial accuracy are used, whereas in e.g. the FEM the distributed loads have to be converted into nodal forces through application of polynomial approximation functions.

6.3. TBL excitation of a clamped plate

In this application case, the geometry and the material properties of the second validation case are reused, see Fig. 10(a) for the geometry and Tab. 1 for the properties of aluminium. The 2 mm thin plate is again clamped on all four edges. The TBL wall pressure is described by the Corcos model (36), with $\alpha = 0.116$, $\beta = 0.7$ the conventional correlation parameters taken from literature [46, 47, 48], and $A(\omega) = 1$ and different values for the convection velocity U_c (in the x-direction). The cross-spectral density of the out-of-plane deformation velocity is calculated and averaged over $n = 384$ response points over the frequency band 50-1000 Hz. The simulations were done using the WBM with a truncation factor of $T = 2$ and the standard setting $T_F = T$ was used for the wavenumber domain truncation (see also Sec. 4.2.2). This results in 48 wave functions and 153 plane waves at 50 Hz and 176 wave functions and 1653 plane waves at 1000 Hz.

Figure 17 shows the resulting cross-spectral density of the deformation velocity for three different convection velocities $U_c = 40, 80, 160$ m/s. Firstly note that for the three considered convection velocities all the resonances of the plate are efficiently excited by this broadband excitation. A second interesting phenomenon can be seen when comparing between different convection velocities. Indeed, an effect known as convective coincidence [49] occurs in all three cases, but at a different

frequency, which can be calculated as:

$$f_{c,con} = \frac{U_c^2}{2\pi}\sqrt{\frac{12\rho(1-\nu^2)}{Et^2}}. \tag{38}$$

This convective coincidence frequency occurs when the convective wavenumber k_c matches the bending wavenumber k_b. In this case the plate is very efficiently excited. The three coincidence frequencies for the studied convective velocities are calculated as $83,330$ and 1322 Hz and are indicated by the vertical lines in Fig. 17. Above this frequency, the response diminishes with 9 dB/octave, as predicted by the asymptote for $k_c \to \infty$ of the Corcos model expression (36), here indicated by the dashed line (– – –). The response thus shows the typical frequency behaviour of a TBL, filtered with the dynamic behaviour of the plate.

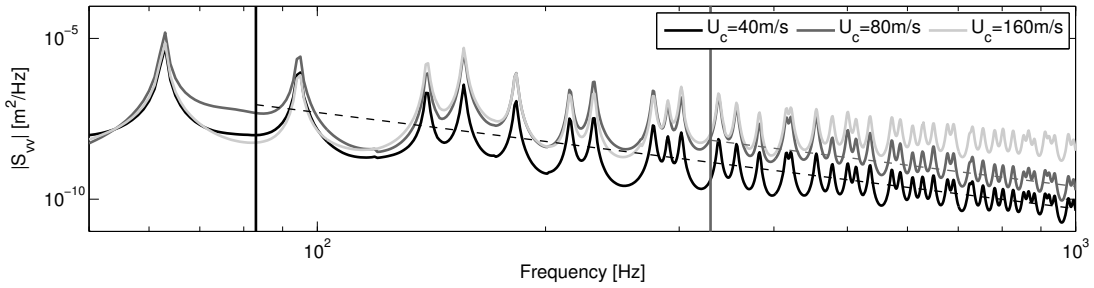

Figure 17: Averaged cross-spectral density of the out-of-plane deformation velocity S_{vv} in $n = 384$ uniformly distributed points from 50 Hz to 1000 Hz for a TBL wall pressure excitation with varying convection velocity $U_c = 40, 80, 160$ m/s.

7. Conclusions

This paper presents particular solution functions for the Wave Based Method (WBM) for plate bending problems with distributed loads. By using exact solutions of the governing differential equation as expansion functions for the dynamic variables, the WBM can produce a higher convergence rate than conventional element-based approaches such as the Finite Element Method (FEM). Two strategies for the application of distributed loads are explored. The first one is based on the integration of a number of point forces distributed over the loaded surface. The second strategy derives new particular solution functions based on a decomposition of the distributed load in the wavenumber domain of the applied load profile. For some specific load profiles, this can be done analytically.

The performance of both approaches is validated numerically against the analytical Rayleigh-Ritz method and the FEM. For the particular functions based on the integration of point forces, the convergence rate is not affected by the applied pressure profile. However, since for every point evaluation a surface integration has to be performed, the approach is rather slow. Only in very specific cases, such as a patch load, it can be competitive. For sufficiently smooth distributed loads, the approach based on the decomposition of the distributed load in the wavenumber domain works best. Moreover, when the applied loads are spatially harmonic or uniform functions, this approach even more clearly outperforms the Hankel-based approach since both the forward and the inverse Fourier transformation can be done analytically. The Fourier based approach also proved well suited to tackle problems with random broadband excitations, such as Turbulent Boundary Layer excitation, through a decomposition of the given excitation wavenumber spectrum into a set of uncorrelated plane waves.

Both approaches expand the application range of the WBM for plate bending problems while keeping the beneficial convergence of the WBM, thus outperforming the FEM for simple geometries.

Acknowledgements

The research of Stijn Jonckheere is funded by a Ph.D. grant of the Institute for the Promotion of Innovation through Science and Technology in Flanders (IWT-Vlaanderen). IWT-Vlaanderen is also gratefully acknowledged for their support of the ASTRA research project, the Fund for Scientific Research Flanders (FWO) and the Research Fund KU Leuven for its research support and the European Commission for their support through the ITN Marie Curie project GA-290050 Gresimo and the EID Marie Curie project GA-316422 eLiQuiD.

Appendix A. Analytical solution for a rectangular plate

For a simply supported rectangular plate, an analytical solution can be derived using modal superposition. The natural frequencies ω_{nm} and mode shapes $\Phi_{nm}(\mathbf{r})$ for a simply supported plate are given by [50]:

$$\omega_{nm}^2 = \frac{DL_xL_y}{M}\left(\frac{n^2\pi^2}{L_x^2}+\frac{m^2\pi^2}{L_y^2}\right)^2, \tag{A.1}$$

$$\Phi_{nm}(\mathbf{r}) = \sin\left(\frac{n\pi x}{L_x}\right)\sin\left(\frac{m\pi y}{L_y}\right), \tag{A.2}$$

with $n = 1, 2, \ldots$ and $m = 1, 2, \ldots$ the mode indices in the x- and y-direction respectively and M the total mass of the plate. The displacement field can then be obtained as an infinite series:

$$w_z(\mathbf{r}) = \frac{1}{M} \sum_n \sum_m \Gamma_{nm}(\omega, \mathbf{r}) \Phi_{nm}(\mathbf{r}). \tag{A.3}$$

The modal magnification factor $\Gamma_{nm}(\omega, \mathbf{r})$ can be calculated by introducing the modal expansion (A.3) into the Kirchhoff plate bending equation (1), with $F_z = 0$:

$$\frac{1}{M} \sum_n \sum_m \left[\left(\left(\frac{n\pi}{L_x} \right)^2 + \left(\frac{m\pi}{L_y} \right)^2 \right)^2 - \left(k_b^s \right)^4 \right] \Gamma_{nm}(\omega, \mathbf{r}) \Phi_{nm}(\mathbf{r}) = -\frac{p(\mathbf{r})}{D}. \tag{A.4}$$

Multiplication with $\Phi_{nm}(\mathbf{r})$ and integration over $\Omega = [0, L_x] \cup [0, L_y]$ gives:

$$\begin{aligned} \frac{1}{M} \sum_n \sum_m \left[\left(\left(\frac{n\pi}{L_x} \right)^2 + \left(\frac{m\pi}{L_y} \right)^2 \right)^2 - \left(k_b^s \right)^4 \right] \Gamma_{nm}(\omega, \mathbf{r}) \frac{L_x L_y}{4} &= \int_\Omega -\frac{p(\mathbf{r})}{D} \Phi_{nm}(\mathbf{r}) d\Omega, \\ &= -\frac{P_{nm}(\mathbf{r})}{D}. \end{aligned} \tag{A.5}$$

This leads to the following expression for $\Gamma_{nm}(\omega, \mathbf{r})$:

$$\Gamma_{nm}(\omega, \mathbf{r}) = \frac{4 P_{nm}(\mathbf{r})}{\omega^2 - \omega_{nm}^2}. \tag{A.6}$$

The term $P_{nm}(\mathbf{r})$ depends on the applied pressure load $p(\mathbf{r})$. The expressions for the different load cases are summarised in Tab. A.4.

References

[1] O.C. Zienkiewicz, R. Taylor, J. Zhu, The Finite Element Method: Its basics and fundamentals, 6th edition, Butterworth-Heinemann, 2005.

[2] P. Bouillard, F. Ihlenburg, Error estimation and adaptivity for the finite element method in acoustics: 2D and 3D applications, Comput. Methods Appl. Mech. Engrg. 176 (1999) 147-163.

[3] F. Ihlenburg, I. Babuška, Finite element solution of the Helmholtz equation with high wavenumber Part I: The h-version of the FEM, Comput. Math. Appl. 30 (9) (1995) 9-37.

[4] F. Ihlenburg, I. Babuška, Finite element solution of the Helmholtz equation with high wavenumber Part II: The h-p-version of the FEM, SIAM J. Numer. Anal. 34 (1) (1997) 315-358.

$p(\mathbf{r})$	$P_{nm}(\mathbf{r})$
1 with $a \leq x \leq b \cup c \leq y \leq d$	$\left[\frac{L_x\left(\cos\left(\frac{\pi na}{L_x}\right)-\cos\left(\frac{\pi nb}{L_x}\right)\right)}{\pi n}\right]\cdot\left[\frac{L_y\left(\cos\left(\frac{\pi mc}{L_y}\right)-\cos\left(\frac{\pi md}{L_y}\right)\right)}{\pi m}\right]$
$x \cdot y$	$\left[\frac{L_x^2\left(\sin\left(\pi n\right)-\pi n\cos\left(\pi n\right)\right)}{\pi^2 n^2}\right]\cdot\left[\frac{L_y^2\left(\sin\left(\pi m\right)-\pi m\cos\left(\pi m\right)\right)}{\pi^2 m^2}\right]$
1	$\left(\frac{L_x-L_x\cos\left(\pi n\right)}{\pi n}\right)\cdot\left(\frac{L_y-L_y\cos\left(\pi m\right)}{\pi m}\right)$
$\sin\frac{p\pi x}{L_x}\sin\frac{q\pi y}{L_y}$	$\frac{L_xL_y}{4}\delta_{np}\delta_{mq}$

Table A.4: Relation between the applied pressure load $p(\mathbf{r})$ and its contribution $P_{nm}(\mathbf{r})$ to the modal magnification factor $\Gamma_{nm}(\omega,\mathbf{r})$.

[5] T. Rabczuk, P.M.A. Areias, T. Belytschko, A meshfree thin shell method for nonlinear dynamic fracture. Int. J. Numer. Meth. Eng. 72(5) (2007) 524-548.

[6] T. Rabczuk, P.M.A. Areias, A meshfree thin shell for arbitrary evolving cracks based on an extrinsic basis. Comp. Model. Eng. 16(2) (2006) 115-130.

[7] D. Wang, H. Peng, A Hermite reproducing kernel Galerkin meshfree approach for buckling analysis of thin plates. Comput. Mech. 51 (2013) 1013-1029.

[8] T.Q. Bui, M.N. Nguyen, A novel meshfree model for buckling and vibration analysis of rectangular orthotropic plates. Struct. Eng. Mech. 39 (2011) 579598.

[9] P. Ladevèze, A new computational approach for structure vibrations in the medium frequency range, Compte rendu de l'académie des sciences de Paris, Série IIb 332 (1996) 849–946.

[10] C. Vanmaele, D. Vandepitte, W. Desmet, An efficient wave based prediction technique for plate bending vibrations, Comput. Methods Appl. Mech. Engrg. 196 (2007) 3178-3189.

[11] E. Trefftz, Ein Gegenstück zum Ritzschen Verfahren, In *Proceedings of the 2nd International Congress on Applied Mechanics*, Zurich, Switzerland, pp.131-137, 1926.

[12] B. Pluymers, B. van Hal, D. Vandepitte, W. Desmet, Trefftz-based methods for time-harmonic acoustics, Arch. Comput. Methods Eng., 14 (2007) 343-381.

[13] C. Farhat, I. Harari, U. Hetmaniuk, A discontinuous Galerkin method with Lagrange multipliers for the solution of Helmholtz problems in the mid-frequency regime, Computer Methods in Applied Mechanics and Engineering 192 (2003) 1389–1419.

[14] J. Jirousek, A. Wróblewski, T-elements: State of the art and future trends, Archives of Computational Methods in Engineering 3 (1996) 323–434.

[15] A. Barnett, T. Betcke, Stability and convergence of the method of fundamental solutions for Helmholtz problems on analytic domains, Journal of Computational Physics 227 (2008) 7003–7026.

[16] G. Fairweather, A. Karageorghis, The method of fundamental solutions for elliptic boundary value problems, Advances in Computational Mathematics 9 (1998) 69–95.

[17] P. Rouch, P. Ladevèze, The variational theory of complex rays: a predictive tool for medium-frequency vibrations, Computer Methods in Applied Mechanics and Engineering 192 (2003) 3301–3315.

[18] O. Cessenat, B. Despres, Application of an ultra weak variational formulation of elliptic PDEs to the two-dimensional Helmholtz problem, SIAM Journal on Numerical Analysis 35 (1998) 255–299.

[19] D. B. Cessenat, O., Using plane waves as base functions for solving time harmonic equations with the ultra weak variational formulation, Journal of Computational Acoustics 11 (2003) 227–238.

[20] T. Huttunen, P. Monk, J. Kaipio, Computational aspects of the ultra-weak variational formulation, Journal of Computational Physics 182 (2002) 27–46.

[21] W. Desmet, A wave based prediction technique for coupled vibro-acoustic analysis, KU Leuven, PhD thesis 98D12, Leuven, 1998.

[22] B. Van Genechten, O. Atak, B. Bergen, E. Deckers, S. Jonckheere, J.S. Lee, A. Maressa, K. Vergote, B. Pluymers, D. Vandepitte, W. Desmet. An efficient Wave Based Method for solving Helmholtz problems in three-dimensional bounded domains. Eng. Anal. Bound. Elem. 36 (2012) 63-75.

[23] B. Bergen, B. Van Genechten, D. Vandepitte, W. Desmet. An efficient Trefftz-based method for three-dimensional Helmholtz problems in unbounded domains. CMES - Comp. Model. Eng. 61 (2010) 155-175.

[24] B. Bergen, B. Pluymers, B. Van Genechten, D. Vandepitte, W. Desmet. A Trefftz based method for solving Helmholtz problems in semi-infinite domains. Eng. Anal. Bound. Elem. 36 (2012) 30-38.

[25] C. Vanmaele, K. Vergote, D. Vandepitte, W. Desmet. Simulation of in-plane vibrations of 2D structural solids with singularities using an efficient wave based prediction technique. Comp. Ass. Mech. Eng. Sc. 19 (2012) 135-171.

[26] E. Deckers, N.E. Hörlin, D. Vandepitte, W. Desmet, A Wave Based Method for the efficient solution of the 2D poroelastic Biot equations, Comput. Methods Appl. Mech. Engrg. 201-204 (2012) 245-262.

[27] E. Deckers, D. Vandepitte, W. Desmet, A Wave Based Method for the axisymmetric dynamic analysis of acoustic and poroelastic problems, Comput. Methods Appl. Mech. Engrg. 257 (2013) 1-16.

[28] B. Van Genechten, D. Vandepitte, W. Desmet, A direct hybrid Finite Element - Wave based modelling technique for efficient coupled vibro-acoustic analysis, Comput. Methods Appl. Mech. Engrg. 200 (2011) 742-764.

[29] S. Jonckheere, E. Deckers, B. Van Genechten, D. Vandepitte, W. Desmet, A direct hybrid Finite Element - Wave Based Method for the steady-state analysis of acoustic cavities with poro-elastic damping layers using the coupled Helmholtz-Biot equations. Comput. Methods Appl. Mech. Engrg. 263 (2013) 144-157.

[30] C. Vanmaele, D. Vandepitte, W. Desmet, An efficient wave based prediction technique for dynamic plate bending problems with corner stress singularities, Comput. Methods Appl. Mech. Engrg. 198 (2009) 2227-2245.

[31] C. Maury, P. Gardiano, S.J. Elliott, A wavenumber approach to modelling the response of a randomly excited panel, Part I: General theory, J. Sound Vib. 252 (2002), 83-113.

[32] G.M. Corcos, Resolution of pressure in turbulence, J. Acoust. Soc. Am. 35 (1963), 192-199.

[33] B.M. Efimtsov, Characteristics of the field of turbulent wall pressure fluctuations at large Reynolds numbers, Soviet Physics–Acoustics 28 (1982), 289-292.

[34] D.M. Chase, Modelling the wavevector-frequency spectrum of turbulent boundary layer wall pressure, J. Sound Vib. 70 (1980), 29-67.

[35] C. Maury, P. Gardiano, S.J. Elliott, A wavenumber approach to modelling the response of a randomly excited panel, Part II: Application to aircraft panels excited by a turbulent boundary layer, J. Sound Vib. 252 (2002), 115-139.

[36] M.K. Bull, Wall-pressure fluctuations beneath turbulent boundary layers: Some reflections on forty years of research, J. Sound Vib. 190 (1996), 299-315.

[37] J. Jegorovs, On hidden Potentials of the wave based method, In *Proceedings of the International Conference on Noise and Vibration Engineering 2010 (ISMA2010)*, Leuven (Belgium), pp. 2361-2370, 2010.

[38] A. Leissa, Vibration of plates, Acoustical Society of America, Woodbury, New York, 1993.

[39] C. Vanmaele, Development of a wave based prediction technique for the efficient analysis of low- and mid-frequency structural vibrations, KU Leuven, division PMA, PhD. thesis 2007D11, 2007.

[40] K. Vergote, Dynamic analysis of structural components in the mid frequency range using the Wave Based Method, KU Leuven, division PMA, PhD. thesis 2012D03, Leuven, 2012.

[41] K. Vergote, D. Vandepitte, W. Desmet, Application of the Wave Based Method for the calculation of structural intensity and power flow in plates, In *Proceedings of the International Conference on Noise and Vibration Engineering 2008 (ISMA2008)*, Leuven (Belgium), pp. 1653-1666, 2008.

[42] L.W. Couch, Digital and Analog Communication Systems, Prentice Hall Engineering/Science/Mathematics, 1997.

[43] H. Nyquist, Certain topics in telegraph transmission theory, AIEE Trans., 47 (1928) 617-644.

[44] L. Cremer, M. Heckl, E. E. Ungar, Structure-borne sound: structural vibrations and sound radiation at audio frequencies. Springer verlag, Berlin, 1973.

[45] P.J. Davis, P. Rabinowitz, Methods for numerical integration, Academic Press Inc., London, 1984.

[46] M. Aucejo, L. Maxit, J.-L. Guyader, Experimental simulation of turbulent boundary layer induced vibrations by using a synthetic array, J. Sound Vib. 331 (221), 3824-3843.

[47] F. Birgersson, N.S. Ferguson, S. Finnveden, Application of the Spectral Finite Element Method to turbulent boundary layer induced vibrations of plates, J. Sound Vib. 259 (2003), 873-891.

[48] S. De Rosa, F. Franco, Exact and numerical response of a plate under a turbulent boundary layer excitation, J. Fluids Structures 24 (2008), 212-230.

[49] G. Robert, Modélisation et simulation du champ excitateur induit sur une structure par une couche limite turbulente, Ecole Centrale de Lyon, PhD thesis 84-02, Lyon, 1984.

[50] E. Skudrzyk, Simple and Complex Vibratory Systems, University Park and London: The Pennsylvania State University Press, 1968.